Original Article | Musculoskeletal Imaging

http://dx.doi.org/10.3348/kjr.2015.16.5.1086
pISSN 1229-6929 · eISSN 2005-8330
Korean J Radiol 2015;16(5):1086-1095

Korean Journal of Radiology
KJR

Comparison of Multi-Echo Dixon Methods with Volume Interpolated Breath-Hold Gradient Echo Magnetic Resonance Imaging in Fat-Signal Fraction Quantification of Paravertebral Muscle

Yeon Hwa Yoo, MD[1], Hak-Sun Kim, MD, PhD[2], Young Han Lee, MD, PhD[3], Choon-Sik Yoon, MD, PhD[1], Mun Young Paek, MS[4], Hanna Yoo, PhD[5], Stephan Kannengiesser, PhD[6], Tae-Sub Chung, MD, PhD[1], Ho-Taek Song, MD, PhD[3], Jin-Suck Suh, MD, PhD[3], Sungjun Kim, MD, PhD[1]

Departments of [1]Radiology and [2]Orthopedic Surgery, Gangnam Severance Hospital, Yonsei University College of Medicine, Seoul 06273, Korea; [3]Department of Radiology, Severance Hospital, Yonsei University College of Medicine, Seoul 03722, Korea; [4]Healthcare Sector, Siemens Ltd., Seoul 03737, Korea; [5]Biostatistics Collaboration Lab, Yonsei University College of Medicine, Seoul 03722, Korea; [6]Healthcare Sector, Siemens AG, Erlangen 91052, Germany

Objective: To assess whether multi-echo Dixon magnetic resonance (MR) imaging with simultaneous T2* estimation and correction yields more accurate fat-signal fraction (FF) measurement of the lumbar paravertebral muscles, in comparison with non-T2*-corrected two-echo Dixon or T2*-corrected three-echo Dixon, using the FF measurements from single-voxel MR spectroscopy as the reference standard.

Materials and Methods: Sixty patients with low back pain underwent MR imaging with a 1.5T scanner. FF mapping images automatically obtained using T2*-corrected Dixon technique with two (non-T2*-corrected), three, and six echoes, were compared with images from single-voxel MR spectroscopy at the paravertebral muscles on levels L4 through L5. FFs were measured directly by two radiologists, who independently drew the region of interest on the mapping images from the three sequences.

Results: A total of 117 spectroscopic measurements were performed either bilaterally (57 of 60 subjects) or unilaterally (3 of 60 subjects). The mean spectroscopic FF was 14.3 ± 11.7% (range, 1.9–63.7%). Interobserver agreement was excellent between the two radiologists. Lin's concordance correlation between the spectroscopic findings and all the imaging-based FFs were statistically significant ($p < 0.001$). FFs obtained from the T2*-corrected six-echo Dixon sequences showed a significantly better concordance with the spectroscopic data, with its concordance correlation coefficient being 0.99 and 0.98 ($p < 0.001$), as compared with two- or three-echo methods.

Conclusion: T2*-corrected six-echo Dixon sequence would be a better option than two- or three-echo methods for noninvasive quantification of lumbar muscle fat quantification.

Index terms: *Magnetic resonance imaging; Fat-signal fraction; Dixon; Muscle; Spine*

INTRODUCTION

The association between chronic low back pain and morphologic, structural changes of the paravertebral muscles has been widely acknowledged (1-4). Considerable research effort has been directed at investigating the fatty infiltration of the paravertebral muscle, as well as the reduction of muscle volume, as a clinical predictor of post-

Received January 26, 2015; accepted after revision May 19, 2015.
This research was supported by the Basic Science Research Program through the National Research Foundation (NRF) of Korea funded by the Ministry of Education, Science and Technology (NRF-2012R1A1A2007991).
Corresponding author: Sungjun Kim, MD, PhD, Department of Radiology, Gangnam Severance Hospital, 211 Eonju-ro, Gangnam-gu, Seoul 06273, Korea.
• Tel: (822) 2019-3510 • Fax: (822) 3462-5472 • E-mail: agn70@yuhs.ac

Korean Journal of Radiology
KJR

surgical outcome (5) and spinal stability (6). Additionally, fatty infiltration of the muscle can also be caused by chronic conditions such as age-related sarcopenia (7), which is the generalized gradual loss of skeletal muscle mass and strength; it is associated to functional limitation, physical disability, and muscle strength (8, 9). Thus, the accurate quantitative measurement of paravertebral muscle fat is an important issue. Magnetic resonance (MR) imaging, which has been investigated for its ability to quantify fat by measuring fat-signal fraction (FF) in various tissues (10-13), is useful for this purpose.

Prior studies have demonstrated that MR imaging techniques involving the quantitative assessment of FF using Dixon technique (14, 15) with two-echo (16) and three-echo (10, 11, 17) in phantom and variable tissues (mostly in the liver) are accurate tools (18). Recently however, FF measurement using multi-echo Dixon techniques have been developed to further improve the accuracy of this approach (19-23). However, there is still no consensus on whether signal acquisition at more echo time points, with or without T2*-correction, would result in more accurate FF measurement of the skeletal muscle.

Therefore, the purpose of our study was to assess whether T2*-corrected multi-echo acquisition allows for a more accurate FF measurement of the paravertebral muscle in comparison with FFs derived from non-T2*-corrected two-echo Dixon or T2*-corrected three-echo Dixon, using FF measurements from single-voxel MR spectroscopy (MRS) as the reference standard.

MATERIALS AND METHODS

Patient Population

This prospective study was approved by our Institutional Review Board prior to patient recruitment. Written informed consent was obtained before the enrollment of each patient. Between June 2013 and October 2013, 60 consecutive patients (39 women, 21 men; mean age: 54.3 ± 19.1 years; age range: 20–92 years) were included in this study. Inclusion criteria were: 1) age greater than 18 years, 2) agreement to participate in the study, and 3) a history of chronic low back pain for more than 3 months. Patients who refused to enroll in the study, those who were claustrophobic, had a cardiac pacemaker, and/or a history of spinal surgery or metallic implant placement, were excluded.

MR Imaging Acquisition

All MR imaging procedures were performed with a 1.5T MR imaging scanner (MAGNETOM Avanto, Siemens Healthcare, Erlangen, Germany) using an integrated spine matrix coil.

All subjects underwent the standard clinical MR imaging protocol at our institution, including T1-weighted turbo-spine echo (TSE) imaging in the sagittal plane, and T2-weighted TSE imaging in the axial and sagittal planes. Imaging parameters for this routine protocol are summarized in Table 1. Next, three different MR imaging pulse sequences for FF quantification were performed using prototype multi-echo three-dimensional gradient echo sequences with inline reconstruction (VIBE-Dixon, work-in-progress #432 for two-echo and three-echo, work-in-progress #798B for six-echo, Siemens Healthcare, Erlangen, Germany). The pulse sequences sampled two, three, and six echoes, respectively. T2*-corrected FF calculation was performed for three- and six-echo data, whereas T2*-correction was not possible for two-echo VIBE-Dixon sequence inherently. For the three-echo acquisitions, T2* was estimated in a first step by a log-linear fit from the

Table 1. Summary of MR Imaging Parameters for Routine Protocol

Imaging Parameters	T1-Weighted TSE Imaging in Sagittal Plane	T2-Weighted TSE Imaging in Axial Plane	T2-Weighted TSE Imaging in Sagittal Plane
Repetition time (ms)	450	3430	3760
Echo time (ms)	9.8	120	100
Echo train length	3	17	20
Receiver bandwidth (Hz/pixel)	162	130	203
Number of excitations	2	3	4
Matrix size	314 x 448	235 x 384	338 x 512
Field of view (mm)	350	220	350
Section thickness (mm)	3	4	3
Slice spacing	3.15	4.4	3.15
Number of slices	17	26	17

TSE = turbo-spin echo

two in-phase echoes. The first opposed-phase and the first in-phase echoes were then T2*-corrected, prior to 2-point Dixon water/fat separation and FF calculation. For the six-echo acquisitions, a multi-step adaptive fitting approach was performed with the technique described in a previous study (24), using a single peak fat model. This was because we could not guarantee that a multiple peak fat model, which has previously been tested in the liver, would be appropriate for the paravertebral muscle.

Images from the protocols were obtained at levels L4 through L5 of the spine, in the axial plane. All fat and water signal-only images with T2* (three- and six-echo) or without T2* (two-echo) images were consequentially reconstructed, thereby automatically generating axial FF mapping images from non-T2*-corrected two-echo VIBE-Dixon, T2*-corrected three-echo VIBE-Dixon, and T2*-corrected six-echo VIBE-Dixon sequences. FFs were calculated with the equation, fat signal / (water signal + fat-signal), using the signal contributions from water and fat obtained in FF mapping images. The imaging time was 51 seconds for non-T2*-corrected two-echo, 86 seconds for T2*-corrected three-echo, and 161 seconds for T2*-corrected six-echo VIBE-Dixon sequence. The imaging parameters of these three pulse sequences are summarized in Table 2.

A flip angle of 5° was used to minimize T1-relaxation effects, which affects the error in fat quantification and is influenced by the difference in T1 values between fat and water when gradient-echo pulse sequences are used (25, 26). As the reference standard, T2-corrected single-voxel multi-echo ^{1}H MRS (HISTO; High speed T2-corrected multiple echo ^{1}H MRS-Fat and R2 Quantification, work-in-progress #599B, Siemens Healthcare) (9) was performed using stimulated echo acquisition mode, with the following parameters: repetition time = 3000 ms, echo time (TE) = 12, 24, 36, 48, and 72 ms, 1024 acquired points, bandwidth = 1200 Hz, voxel size = 15 x 15 x 15 mm^3. The acquisition duration for the HISTO sequence was 15 seconds.

A spectroscopic voxel was placed in either the lumbar erectus spinae muscle or lumbar multifidus muscle, at any random level between the L4 and L5 vertebral bodies, and repeated in the contralateral side in every subject. The voxel was placed by an MR imaging technician under the supervision of a musculoskeletal radiologist, who had around 30 years of experience in the field of musculoskeletal radiology. We focused on the lumbar erectus spinae muscles and lumbar multifidus muscles, which are known to be important stabilizers of the lumbar spine (27) at levels L4 and L5; this selection was based on an earlier study that demonstrated that the paravertebral muscle fat at the L4 through L5 levels could be a useful marker of whole body skeletal muscle fat (28). Based on the signals from fat and water at each TE, FF was automatically calculated from this sequence. An example of the spectral peaks at a certain TE and the automatically calculated FF from the HISTO sequence is demonstrated in Figure 1.

Image Analysis

Fat-signal fraction from the mapping images were

Table 2. Summary of MR Imaging Parameters for Fat-Signal Fraction Measurement Pulse Sequences

Imaging Parameters	Non-T2*-Corrected Two-Echo VIBE-Dixon	T2*-Corrected Three-Echo VIBE-Dixon	T2*-Corrected Six-Echo VIBE-Dixon
Repetition time (ms)	6.96	11.7	16.6
Echo time (ms)	2.38 (TE1) 4.76 (TE2)	2.38 (TE1) 4.76 (TE2) 9.52 (TE3)	2.39 (TE1) 4.78 (TE2) 7.17 (TE3) 9.56 (TE4) 11.95 (TE5) 14.34 (TE6)
Flip angle (°)	5	5	5
Section thickness (mm)	3	3	3
Matrix size	160 x 160	160 x 160	160 x 160
Field of view (mm)	250	250	250
NEX (n)	2	2	2
Voxel resolution (mm)	1.6 x 1.6 x 3.0	1.6 x 1.6 x 3.0	1.6 x 1.6 x 3.0
Imaging time (s)	51	86	161

NEX = number of excitations, TE = echo time, TE1, TE2, TE3, TE4, TE5, TE6 = TE at each echo point, VIBE = volume interpolated breath-hold gradient echo

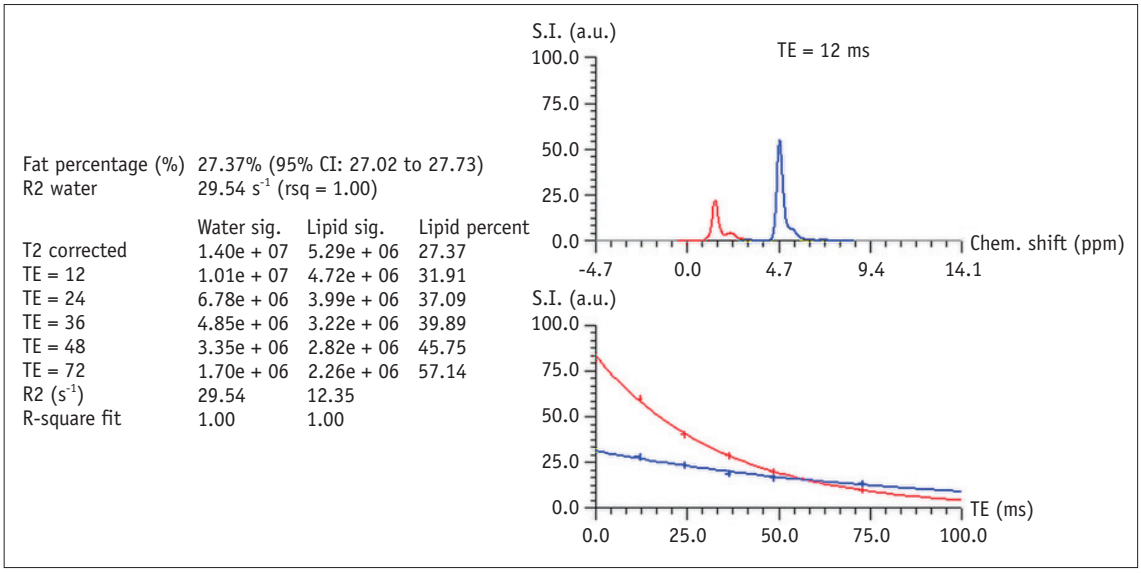

Fig. 1. T2-corrected single-voxel multi-echo ^{1}H MR spectroscopy (MRS). Screen-captured image of T2-corrected single-voxel multi-echo ^{1}H MRS result from 62-year-old female subject. Data on left includes five water and fat integrals at each measured echo (TE = 12, 24, 36, 48, and 72 ms) and estimated fat-signal fraction was 27.4%. Image on top right shows representative water and fat spectral peaks, which were measured at TE of 12 ms. Image on bottom left shows T2 exponential decay. CI = confidence interval, TE = echo time

measured by drawing a circular region of interest (ROI) at the MR imaging workstation (VB17, Siemens Healthcare) using Syngo software. After randomization of the subjects, two musculoskeletal radiologists (observer A, observer B) performed all measurements independently, without knowledge of the FF measurements from the MRS. ROIs were drawn on a mapping image from the two-echo sequence, at the same location of the spectroscopic voxel that referred to the captured images obtained while placing the voxel in each instance of MR imaging. These were then copied and pasted to two other mapping images (Fig. 2). The diameter of the circular ROI was fixed at 15 mm, based on the voxel size of MRS. For precise representative data acquisition over the entire voxel area, ROIs were drawn at the three consecutive slices of mapping images in the same manner as stated above. As a result, three ROI measurements from the three FF pulse sequences were obtained for every voxel location.

Statistical Analysis

All continuous data were expressed as mean ± standard deviation values. The intraclass correlation coefficient (ICC), with a two-way random model of absolute agreement, was used to evaluate the agreement of FF measurements between the two radiologists (observer A and B). For interpretations of the results, ICC values less than 0.40 indicate poor reproducibility, ICC values in the range of 0.40 to 0.75 indicate fair to good reproducibility, and ICC values greater than 0.75 indicate excellent reproducibility (29).

To determine the agreement between the FF measurements obtained from the FF maps from VIBE-Dixon sequences and those obtained using MRS, Lin's concordance correlation coefficient (CCC) was used (30). Accordingly, three CCCs for the VIBE-Dixon sequences were obtained for measurements by each observer. Subsequently, multiple comparisons with Streiger's Z-test was done as post-hoc analysis through a Bonferroni correction by using the aforementioned CCCs, to determine if there was a significant difference between the results obtained from the three different VIBE-Dixon MR sequences, with an adjusted significance level (0.05/3).

In order to show the mean measurement bias (mean difference) with corresponding limits of agreement of the FF measurements obtained from the three different VIBE-Dixon sequences and those from MRS, Bland-Altman analysis was used with a 95% confidential interval (31). All statistical analyses were performed using statistical software (SAS Institute, version 9.2, Cary, NC, USA).

RESULTS

A total of 120 spectroscopic FF measurements were done. Of these, 117 spectroscopic FF measurements were completed either bilaterally (57 of 60) or unilaterally (3 of 60), and the values were used as reference standards. Three MRS data from three subjects were missed owing to a storage error while saving the result; hence, the

measurements from the remaining 117 sites were assessed.

The mean spectroscopic FF percentage was 14.3 ± 11.7% (range, 1.9–63.7%). The mean FFs from each VIBE-Dixon sequence obtained by observers A and B are summarized in Table 3. The interobserver agreement for the FF measurements between observers A and B was excellent for all three VIBE-Dixon sequences (Table 4).

Lin's CCCs between the spectroscopic and all the imaging-based FFs were statistically significant ($p < 0.001$) (Fig. 3). The CCCs for each VIBE-Dixon sequence in observer A and B are summarized in Table 4.

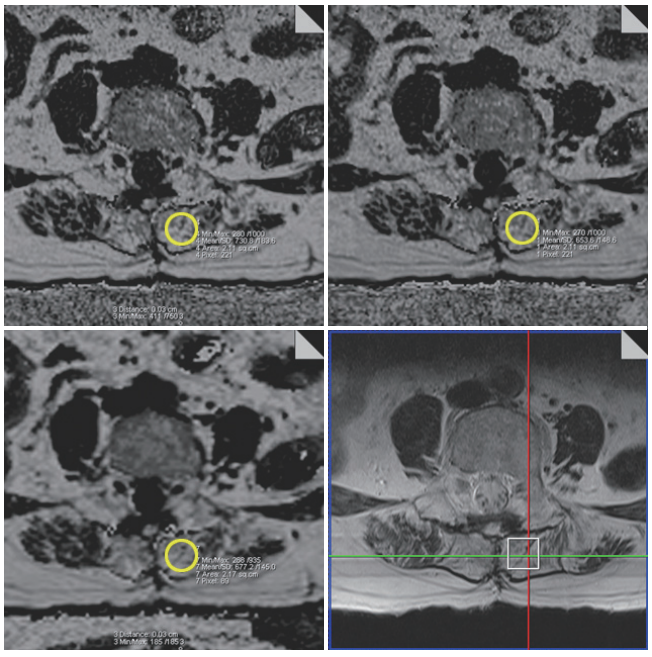

Fig. 2. Region of interest (ROI) placement from mapping images. Example of screen-captured image of ROI placement from mapping images, obtained from 68-year-old male subject. ROI was drawn on mapping image from non-T2*-corrected two-echo volume interpolated breath-hold gradient-echo Dixon (VIBE-Dixon) sequence (top left) at same location of spectroscopic voxel referring to captured image (bottom right) obtained while placing voxel in each MR imaging. This was then copied and pasted to other mapping images from T2*-corrected three-echo VIBE-Dixon sequence (top right) and T2*-corrected six-echo VIBE-Dixon sequence (bottom right). Diameter of circular ROI was fixed at 15 mm, based on voxel size of MR spectroscopy. For precise representative data acquisition embracing entire voxel area, ROIs were drawn at three consecutive slices of mapping images in same manner as stated above. As result, three ROI measurements from three fat-signal fraction pulse sequences were obtained for every voxel location.

As compared with the other imaging-based FFs through multiple comparisons, the FF obtained from T2*-corrected six-echo VIBE-Dixon sequence showed the best agreement with the spectroscopic data, and was statistically significant ($p < 0.001$). However, there was no statistically significant difference between non-T2*-corrected two-echo VIBE-Dixon and T2*-corrected three-echo VIBE-Dixon in observer A ($p = 0.44$) or observer B ($p = 0.84$).

Figure 4 shows the mean measurement bias with corresponding limits of agreement for FFs obtained from three different VIBE-Dixon sequences and those from MRS. The mean measurement bias was -2.5% (range, -9.2% to 4.2%) for two-echo, -2.4% (range, -8.6% to 3.7%) for three-echo, and 0.2% (range, -2.8% to 3.3%) for six-echo methods as evaluated by observer A, and -2.6% (range, -9.0% to 3.9%) for two-echo, -3.1% (range, -9.4% to 3.3%) for three-echo, and 0.5% (range, -2.9% to 3.9%) for six-echo methods as evaluated by observer B. In the findings of each observer, the range of limits of agreement was very narrow for T2*-corrected six-echo VIBE-Dixon findings, in comparison with the other sequences.

DISCUSSION

We attempted to validate whether T2*-correction, based on signals from multiple TE, helps to increase the accuracy in the measurement of FF, especially for paravertebral skeletal muscle. Several researchers have focused on quantification of skeletal muscle fat by MR imaging in various parts of the body, including the rotator cuff (12, 32), thigh (25), and paravertebral muscles (33) using Dixon technique with or without T2*-correction. However, to the best of our knowledge, our research is the first one that demonstrates that FF obtained by T2*-corrected six-echo VIBE-Dixon best correlates with MR spectroscopic FF data, in comparison with inherently non-T2*-corrected two-echo VIBE-Dixon and T2*-corrected three-echo VIBE-Dixon data.

Most of the previous FF studies in the liver have already shown that T2*-correction generally improves the accuracy

Table 3. Comparison between Mean Values of Fat-Signal Fraction Derived from VIBE-Dixon Sequence

	Non-T2*-Corrected Two-Echo VIBE-Dixon	T2*-Corrected Three-Echo VIBE-Dixon	T2*-Corrected Six-Echo VIBE-Dixon
Mean values of FF (%) (observer A)	16.8 ± 12.3 (4.2–77.5)	16.7 ± 11.3 (4.4–69.0)	14.0 ± 11.7 (1.4–64.3)
Mean values of FF (%) (observer B)	16.8 ± 12.6 (4.3–77.3)	17.3 ± 11.7 (4.3–66.5)	13.7 ± 11.5 (1.9–64.6)

All continuous data were expressed as mean value ± standard deviation. Numbers in parentheses are value ranges. FF = fat-signal fraction, VIBE-Dixon = volume interpolated breath-hold gradient echo Dixon sequence

Korean Journal of Radiology
KJR

Table 4. Intraclass Correlation Coefficient (ICC) for Each Observer and Concordance Correlation Coefficient (CCC) between Observers

	Non-T2*-Corrected Two-Echo VIBE-Dixon	T2*-Corrected Three-Echo VIBE-Dixon	T2*-Corrected Six-Echo VIBE-Dixon
ICC* of two observers	0.914	0.918	0.909
CCC† of observer A	0.93	0.94	0.99
CCC‡ of observer B	0.94	0.93	0.98

*ICC was used to evaluate agreement of fat-signal fraction (FF) measurement between two observers (observer A and observer B), †CCC was used to determine agreement between FF obtained from each VIBE-Dixon sequences and FF obtained using MR spectroscopy in observer A, ‡CCC was used to determine agreement between FF obtained from each VIBE-Dixon sequences and FF obtained using MR spectroscopy in observer B. VIBE-Dixon = volume interpolated breath-hold gradient echo Dixon sequence

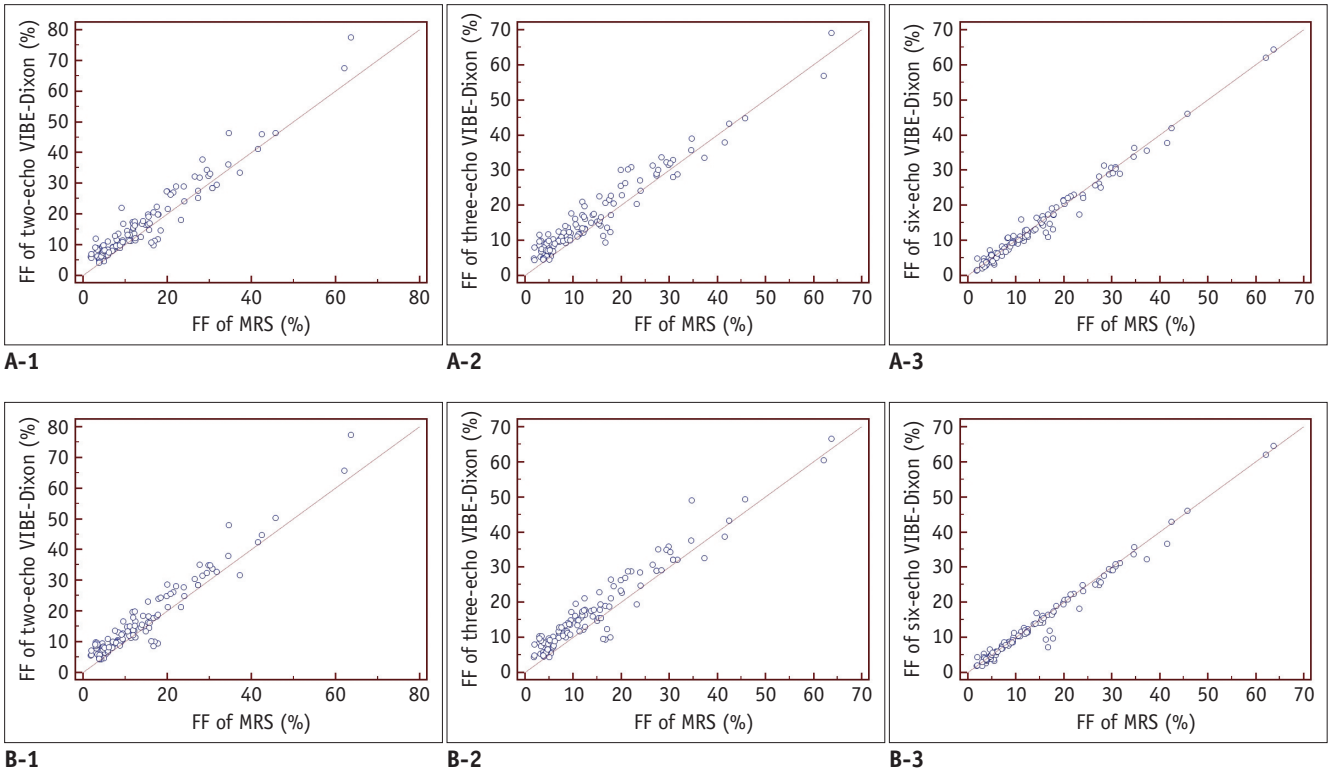

Fig. 3. Concordance correlation coefficient (CCC) of fat-signal fraction (FF) between MR spectroscopy (MRS) and mapping image measurements.

Concordance correlation coefficient for assessment of agreement between MRS and mapping image measurements obtained from FF maps using non-T2*-corrected two-echo VIBE-Dixon sequence (Observer A, **A-1**; Observer B, **B-1**), T2*-corrected three-echo Dixon sequence (Observer A, **A-2**; Observer B, **B-2**), T2*-corrected six-echo VIBE-Dixon sequence (Observer A, **A-3**; Observer B, **B-3**) in each observer. Correlation of FFs between all mapping images and spectroscopic data was statistically significant in each observer ($p < 0.001$). CCC was 0.93 for two-echo VIBE-Dixon, 0.94 for three-echo VIBE-Dixon, 0.99 for six-echo VIBE-Dixon pulse sequence in observer A, and was 0.94 for two-echo VIBE-Dixon, 0.93 for three-echo VIBE-Dixon, and 0.98 for six-echo VIBE-Dixon pulse sequence in observer B. FF of two-echo = FF obtained from non-T2*-corrected two-echo VIBE-Dixon sequence, FF of three-echo = FF obtained from T2*-corrected three-echo VIBE-Dixon sequence, FF of six-echo = FF obtained from T2*-corrected six-echo VIBE-Dixon sequence, FF of MRS = FF obtained from MR spectroscopy, VIBE-Dixon = volume interpolated breath-hold gradient-echo Dixon

of FF measurement in three or more TEs using multi-echo VIBE-Dixon technique (34-37). Previous studies on the liver have also established that three-echo VIBE-Dixon shows a more accurate measurement in the assessment of hepatic FF than two-echo VIBE-Dixon, and that six-echo VIBE-Dixon shows a more accurate measurement than three-echo VIBE-Dixon (34, 38). We have confirmed that the correlation between spectroscopic data and all imaging-based FFs was statistically significant, which was consistent with the results of a previous investigation, that assessed the FFs of lumbar paravertebral muscles from three different gradient echo sequences based on Dixon techniques using non-T2*-corrected two-echo, T2*-corrected multi-echo, and non-T2*-corrected multi-echo (33). However, Fischer

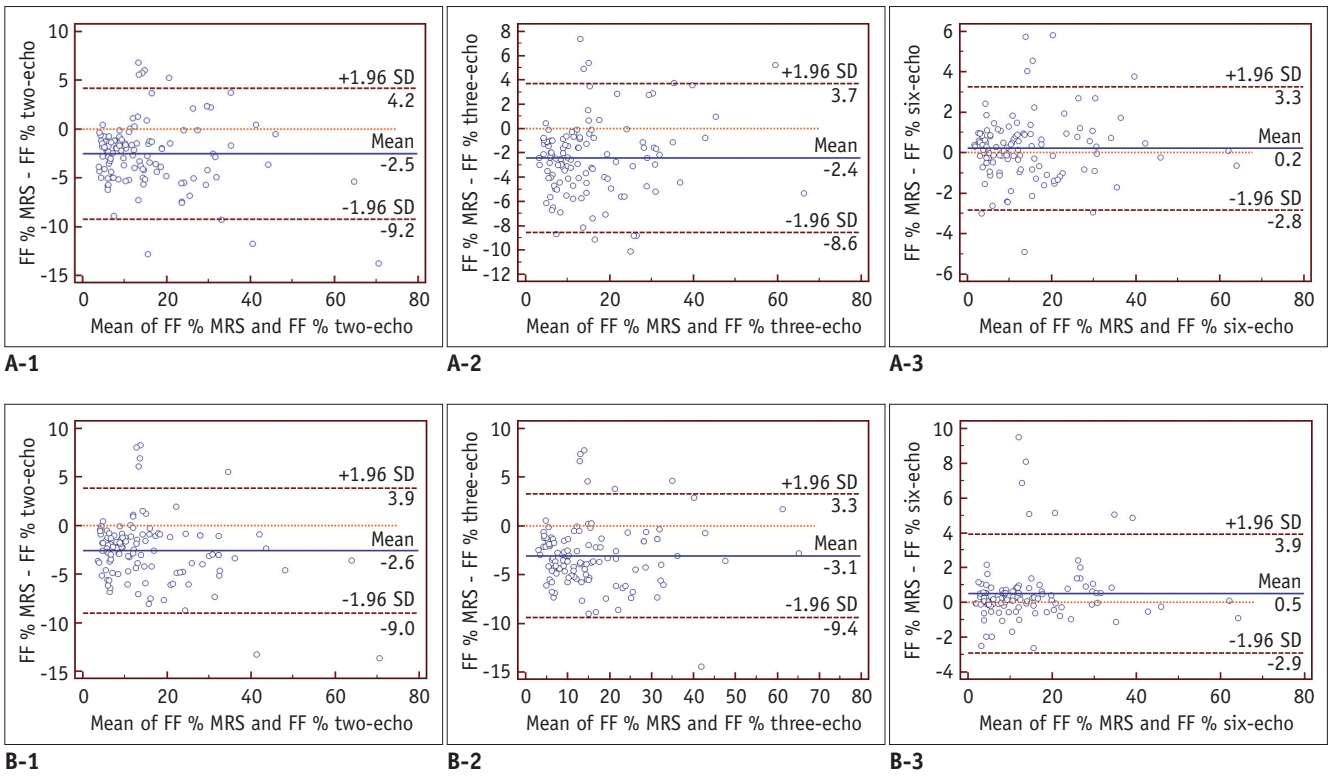

Fig. 4. Bland-Altman plots for assessment of agreement of fat-signal fraction (FF) between MR spectroscopy (MRS) and mapping image measurements.

Bland-Altman plot shows mean measurement bias with limits of agreement of FFs, obtained from FF maps using non-T2*-corrected two-echo volume interpolated breath-hold gradient-echo (VIBE-Dixon) sequence (Observer A, **A-1**; Observer B, **B-1**), T2*-corrected three-echo VIBE-Dixon sequence (Observer A, **A-2**; Observer B, **B-2**), and T2*-corrected six-echo VIBE-Dixon sequence (Observer A, **A-3**; Observer B, **B-3**) in relation to FFs measured with MRS. Narrow range of limits of agreement was seen in T2*-corrected six-echo VIBE-Dixon as compared with other sequences in each observer. FF % two-echo = FF obtained from non-T2*-corrected two-echo VIBE-Dixon sequence, FF % three-echo = FF obtained from T2*-corrected three-echo VIBE-Dixon sequence, FF % six-echo = FF obtained from T2*-corrected six-echo VIBE-Dixon sequence, FF % MRS = FF obtained from MR spectroscopy, SD = standard deviation

et al. (33) unexpectedly found that T2*-correction was not helpful. They demonstrated that the T2*-corrected multi-echo sequence data did not correlate better with FF data from spectroscopy, than the non-T2*-corrected multi-echo sequence did; they hypothesized that this could be owing to the reduction of the signal-to-noise ratio caused by T2*-correction. Another report from Gaeta et al. (19) had explained that T2*-correction had no more benefit than non-T2*-corrected method in skeletal muscle than for tissues with a longer T2*, referring that the T2* of muscle is around 30 ms.

Although the necessity of T2*-correction in the assessment of skeletal muscle fat has not been established, we employed T2*-correction for three-echo and six-echo VIBE-Dixon sequences from the commencement of our study, based on the hypothesis that there are potential factors that can cause T2* decay in muscle. It is well known that the cause of T2* decay in hepatic parenchyma can mainly be explained by the incidence of iron (39). Theoretically, there are non-negligible amounts of iron stored in skeletal muscle that can affect the local magnetic inhomogeneity in the muscle, as is the case in the liver (40). Recent studies, however, have revealed that iron also plays an important role in muscle atrophy (41) and in the development of sarcopenia (42). This process can be more complex in the paravertebral muscles of patients with chronic low back pain when combined with microstructural changes of muscle fiber type (4) and changes of muscle fiber stiffness (43). We believe that such changes should not be neglected in the skeletal muscle, which may influence the local magnetic inhomogeneity, although the influence can be subtle with individual variances.

It is noteworthy that a prior phantom study assessed FF with fat-water-iron phantom using T2*-corrected multi-echo chemical shift-based method, with a variable iron concentration (37). This phantom study demonstrated the necessity of T2*-correction in six-echo chemical shift-based fat-water separation method, regardless of the iron

Korean Journal of Radiology
KJR

concentration (0–50 μg/mL), particularly in conditions with FF lower than 50%. Since most of the observed FFs were lower than 50% in the present study, we assumed that T2*-correction could be helpful in the accurate measurement of muscle FF, even without knowing the exact iron concentration in muscle. Accordingly, our study result with T2*-corrected six-echo sequence has confirmed the prior phantom study result *in vivo*, particularly in the skeletal muscle.

In this study, the narrow range of limits of agreement in T2*-corrected six-echo VIBE-Dixon data was small enough to explain the more precise correlation with FF derived from MRS according to Bland-Altman analysis. Underestimation of FF measurement was found in all three imaging-based FFs with each observer, but was least prominent in T2*-corrected six-echo sequences. We observed slight errors in the FF measurements in each VIBE-Dixon sequence. However, most of the measurements were within the 95% limits without systematic error in the assessment of FF. For each observer, the smallest mean difference (0.2% in observer A, 0.5% in observer B) was noted in T2*-corrected six-echo VIBE-Dixon, which enhances confidence in this methodology.

We also observed that there was no statistically significant difference between the non-T2*-corrected two-echo VIBE-Dixon and T2*-corrected three-echo VIBE-Dixon sequences. This might have been caused by insufficient T2*-correction in three-echo VIBE-Dixon sequence. Another plausible explanation can be inferred from Reeder et al. (44), who suggested that it is necessary to acquire at least six echoes for the optimal separation of water and fat signals with T2*-correction (20).

Our study has several limitations. First, we used MRS as a reference standard rather than traditional pathologic confirmation by muscle biopsy. However, muscle biopsies cannot always be performed, owing to ethical problems. Additionally, the small portion of muscle gained from a biopsy cannot always represent the whole muscle condition. Secondly, there was a relatively small population of patients with a higher muscle FF (> 50%). Therefore, we still need to elucidate whether this methodology can be applied for patients with massive fat infiltration. Third, our study used single fat-peak spectral modeling for multi-echo VIBE-Dixon MR imaging. It has been suggested by Yokoo et al. (34) that a single fat-peak model could be inadequate for reliable T2* estimation in MRI. However, little has been known about the usefulness of multi-peak fat modeling for muscle FF measurement in comparison with single-peak fat modeling. Therefore, further large-scale studies would be needed, taking into consideration both T2*-correction and multi-peak fat modeling.

In conclusion, T2*-corrected six-echo VIBE-Dixon sequence agrees with spectroscopic FFs better, as compared to non-T2*-corrected two-echo and T2*-corrected three-echo VIBE-Dixon sequences. Based on our observations, T2*-corrected six-echo VIBE-Dixon sequence could be used as an accurate, clinically feasible, noninvasive quantification tool for muscle fat quantification in lumbar spine MR imaging.

REFERENCES

1. Freeman MD, Woodham MA, Woodham AW. The role of the lumbar multifidus in chronic low back pain: a review. *PM R* 2010;2:142-146; quiz 1 p following 167
2. Kjaer P, Bendix T, Sorensen JS, Korsholm L, Leboeuf-Yde C. Are MRI-defined fat infiltrations in the multifidus muscles associated with low back pain? *BMC Med* 2007;5:2
3. Mengiardi B, Schmid MR, Boos N, Pfirrmann CW, Brunner F, Elfering A, et al. Fat content of lumbar paraspinal muscles in patients with chronic low back pain and in asymptomatic volunteers: quantification with MR spectroscopy. *Radiology* 2006;240:786-792
4. Mannion AF. Fibre type characteristics and function of the human paraspinal muscles: normal values and changes in association with low back pain. *J Electromyogr Kinesiol* 1999;9:363-377
5. Hebert JJ, Marcus RL, Koppenhaver SL, Fritz JM. Postoperative rehabilitation following lumbar discectomy with quantification of trunk muscle morphology and function: a case report and review of the literature. *J Orthop Sports Phys Ther* 2010;40:402-412
6. Chan ST, Fung PK, Ng NY, Ngan TL, Chong MY, Tang CN, et al. Dynamic changes of elasticity, cross-sectional area, and fat infiltration of multifidus at different postures in men with chronic low back pain. *Spine J* 2012;12:381-388
7. Cruz-Jentoft AJ, Baeyens JP, Bauer JM, Boirie Y, Cederholm T, Landi F, et al. Sarcopenia: European consensus on definition and diagnosis: Report of the European Working Group on Sarcopenia in Older People. *Age Ageing* 2010;39:412-423
8. Dufour AB, Hannan MT, Murabito JM, Kiel DP, McLean RR. Sarcopenia definitions considering body size and fat mass are associated with mobility limitations: the Framingham Study. *J Gerontol A Biol Sci Med Sci* 2013;68:168-174
9. Pineda-Alonso N, Xu Q, Sharma P, Martin D, Hu X. High speed multiple echo acquisition (HISTO): a rapid and simultaneous assessment of fat and iron content in liver by ^{1}HMRS. *Proc Intl Soc Mag Reson Med* 2008;16:3699
10. Brix G, Heiland S, Bellemann ME, Koch T, Lorenz WJ.

MR imaging of fat-containing tissues: valuation of two quantitative imaging techniques in comparison with localized proton spectroscopy. *Magn Reson Imaging* 1993;11:977-991
11. Kim H, Taksali SE, Dufour S, Befroy D, Goodman TR, Petersen KF, et al. Comparative MR study of hepatic fat quantification using single-voxel proton spectroscopy, two-point dixon and three-point IDEAL. *Magn Reson Med* 2008;59:521-527
12. Nardo L, Karampinos DC, Lansdown DA, Carballido-Gamio J, Lee S, Maroldi R, et al. Quantitative assessment of fat infiltration in the rotator cuff muscles using water-fat MRI. *J Magn Reson Imaging* 2014;39:1178-1185
13. Karampinos DC, Melkus G, Baum T, Bauer JS, Rummeny EJ, Krug R. Bone marrow fat quantification in the presence of trabecular bone: initial comparison between water-fat imaging and single-voxel MRS. *Magn Reson Med* 2014;71:1158-1165
14. Bley TA, Wieben O, François CJ, Brittain JH, Reeder SB. Fat and water magnetic resonance imaging. *J Magn Reson Imaging* 2010;31:4-18
15. Berglund J, Ahlström H, Johansson L, Kullberg J. Two-point dixon method with flexible echo times. *Magn Reson Med* 2011;65:994-1004
16. Fischer MA, Nanz D, Reiner CS, Montani M, Breitenstein S, Leschka S, et al. Diagnostic performance and accuracy of 3-D spoiled gradient-dual-echo MRI with water- and fat-signal separation in liver-fat quantification: comparison to liver biopsy. *Invest Radiol* 2010;45:465-470
17. Bernard CP, Liney GP, Manton DJ, Turnbull LW, Langton CM. Comparison of fat quantification methods: a phantom study at 3.0T. *J Magn Reson Imaging* 2008;27:192-197
18. Hayashi N, Miyati T, Minami T, Takeshita Y, Ryu Y, Matsuda T, et al. Quantitative analysis of hepatic fat fraction by single-breath-holding MR spectroscopy with T_2 correction: phantom and clinical study with histologic assessment. *Radiol Phys Technol* 2013;6:219-225
19. Gaeta M, Scribano E, Mileto A, Mazziotti S, Rodolico C, Toscano A, et al. Muscle fat fraction in neuromuscular disorders: dual-echo dual-flip-angle spoiled gradient-recalled MR imaging technique for quantification--a feasibility study. *Radiology* 2011;259:487-494
20. Yu H, McKenzie CA, Shimakawa A, Vu AT, Brau AC, Beatty PJ, et al. Multiecho reconstruction for simultaneous water-fat decomposition and T2* estimation. *J Magn Reson Imaging* 2007;26:1153-1161
21. Elliott JM, Walton DM, Rademaker A, Parrish TB. Quantification of cervical spine muscle fat: a comparison between T1-weighted and multi-echo gradient echo imaging using a variable projection algorithm (VARPRO). *BMC Med Imaging* 2013;13:30
22. Horng DE, Hernando D, Hines CD, Reeder SB. Comparison of R2* correction methods for accurate fat quantification in fatty liver. *J Magn Reson Imaging* 2013;37:414-422
23. Koelblinger C, Kršśák M, Maresch J, Wrba F, Kaczirek K, Gruenberger T, et al. Hepatic steatosis assessment with 1H-spectroscopy and chemical shift imaging at 3.0 T before hepatic surgery: reliable enough for making clinical decisions? *Eur J Radiol* 2012;81:2990-2995
24. Zhong X, Nickel MD, Kannengiesser SA, Dale BM, Kiefer B, Bashir MR. Liver fat quantification using a multi-step adaptive fitting approach with multi-echo GRE imaging. *Magn Reson Med* 2014;72:1353-1365
25. Wokke BH, Bos C, Reijnierse M, van Rijswijk CS, Eggers H, Webb A, et al. Comparison of dixon and T1-weighted MR methods to assess the degree of fat infiltration in duchenne muscular dystrophy patients. *J Magn Reson Imaging* 2013;38:619-624
26. Liu CY, McKenzie CA, Yu H, Brittain JH, Reeder SB. Fat quantification with IDEAL gradient echo imaging: correction of bias from T(1) and noise. *Magn Reson Med* 2007;58:354-364
27. Ropponen A, Videman T, Battié MC. The reliability of paraspinal muscles composition measurements using routine spine MRI and their association with back function. *Man Ther* 2008;13:349-356
28. Lee SJ, Janssen I, Heymsfield SB, Ross R. Relation between whole-body and regional measures of human skeletal muscle. *Am J Clin Nutr* 2004;80:1215-1221
29. Rosner B. *Fundamentals of biostatistics*. 6th ed. Boston: Duxbury Press, 2005
30. Lin LI. A concordance correlation coefficient to evaluate reproducibility. *Biometrics* 1989;45:255-268
31. Dewitte K, Fierens C, Stöckl D, Thienpont LM. Application of the Bland-Altman plot for interpretation of method-comparison studies: a critical investigation of its practice. *Clin Chem* 2002;48:799-801; author reply 801-802
32. Lee YH, Kim S, Lim D, Song HT, Suh JS. MR Quantification of the Fatty Fraction from T2*-corrected Dixon Fat/Water Separation Volume-interpolated Breathhold Examination (VIBE) in the Assessment of Muscle Atrophy in Rotator Cuff Tears. *Acad Radiol* 2015;22:909-917
33. Fischer MA, Nanz D, Shimakawa A, Schirmer T, Guggenberger R, Chhabra A, et al. Quantification of muscle fat in patients with low back pain: comparison of multi-echo MR imaging with single-voxel MR spectroscopy. *Radiology* 2013;266:555-563
34. Yokoo T, Shiehmorteza M, Hamilton G, Wolfson T, Schroeder ME, Middleton MS, et al. Estimation of hepatic proton-density fat fraction by using MR imaging at 3.0 T. *Radiology* 2011;258:749-759
35. Cassidy FH, Yokoo T, Aganovic L, Hanna RF, Bydder M, Middleton MS, et al. Fatty liver disease: MR imaging techniques for the detection and quantification of liver steatosis. *Radiographics* 2009;29:231-260
36. Bydder M, Yokoo T, Hamilton G, Middleton MS, Chavez AD, Schwimmer JB, et al. Relaxation effects in the quantification of fat using gradient echo imaging. *Magn Reson Imaging* 2008;26:347-359
37. Hines CD, Yu H, Shimakawa A, McKenzie CA, Brittain JH, Reeder SB. T1 independent, T2* corrected MRI with accurate spectral modeling for quantification of fat: validation in a fat-water-SPIO phantom. *J Magn Reson Imaging* 2009;30:1215-1222

38. Kang BK, Yu ES, Lee SS, Lee Y, Kim N, Sirlin CB, et al. Hepatic fat quantification: a prospective comparison of magnetic resonance spectroscopy and analysis methods for chemical-shift gradient echo magnetic resonance imaging with histologic assessment as the reference standard. *Invest Radiol* 2012;47:368-375
39. Westphalen AC, Qayyum A, Yeh BM, Merriman RB, Lee JA, Lamba A, et al. Liver fat: effect of hepatic iron deposition on evaluation with opposed-phase MR imaging. *Radiology* 2007;242:450-455
40. Beard JL. Iron biology in immune function, muscle metabolism and neuronal functioning. *J Nutr* 2001;131(2S-2):568S-579S; discussion 580S
41. Kondo H, Miura M, Kodama J, Ahmed SM, Itokawa Y. Role of iron in oxidative stress in skeletal muscle atrophied by immobilization. *Pflugers Arch* 1992;421:295-297
42. Hofer T, Marzetti E, Xu J, Seo AY, Gulec S, Knutson MD, et al. Increased iron content and RNA oxidative damage in skeletal muscle with aging and disuse atrophy. *Exp Gerontol* 2008;43:563-570
43. Brown SH, Gregory DE, Carr JA, Ward SR, Masuda K, Lieber RL. ISSLS prize winner: adaptations to the multifidus muscle in response to experimentally induced intervertebral disc degeneration. *Spine (Phila Pa 1976)* 2011;36:1728-1736
44. Reeder SB, Robson PM, Yu H, Shimakawa A, Hines CD, McKenzie CA, et al. Quantification of hepatic steatosis with MRI: the effects of accurate fat spectral modeling. *J Magn Reson Imaging* 2009;29:1332-1339